Constraints on Beyond Standard Model vector boson ineractions in an effective field theory using differencial cross section of the production of two jets associate with four charged leptons at $\sqrt{s} = 13$ TeV with the ATLAS detector

---

Dong Qichen

The University of Manchester,
316 Oxford Road, UK

E-mail: dong.qichen@student.manchester.ac.uk

Abstract: In this report, the production of a pair on-shell Z bosons associate with a pair of jets in a electroweak enhanced phase space region was measured at centre-of-mass energy $\sqrt{s} = 13$ TeV with 139 fb^{-1} of pp collision data collected by the ATLAS detector. The result is compatible with the Standard Model prediction. The differencial cross sections as functions of two CP-sensitive observables were obtained by removing the detector effect from the measurement. The differencial measurements were then reinterpreted in a dimention-6 Standard Model Effect Field Theory and constraients on relavent CP-odd and CP-even new physics operators were obtained.

Contents

1 Introduction

The Standard Model of particle physics (SM)[1] has been a very successful theory in predicting the nature of fundamental particles and their interactions, However, the SM is not yet complete, for example, the enormous matter-antimatter asymmetry[2] observed in the universe is not fully described by the SM. Being sensitve to Beyond the SM (BSM) physics is one of the main goal of the Large Hardron Collidor (LHC)[3]. At current energy scale, the BSM effects may manifest themselfs as small corrections to the SM, searching for deviations from the SM prediction therefore a general way to search the new physics phenomena.

Since the discovery of the last particle predicted by the SM, the Higgs boson, in 2012[4], the nature of its interactions with other particles has been carefully investigated in order to seek any deviation from the SM. The Vector Boson Scattering (VBS) process[5], a important pure electroweak process in the LHC, enables us to probe the nature of Higgs boson interactions with vector bosons and to constrain BSM hypothesis altering the nature of the Higgs boson and/or vector bosons which

may provide alternative Electroweak Symmetry Breaking (EWSB) machenism[6] and additional source of CP violation[7].

In the LHC, VBS events are produced by a pair of vector bosons radiated from the colliding partons scattered to another pair of vector bosons subsequently. At the detector-level, the signiture of VBS events are two jets from the initial partons associate with the decay products of two vector boson, we denote such events $VVjj$. The evidence of electroweak production of $W^{\pm}W^{\pm}jj$ ($EWW^{\pm}W^{\pm}jj$) was first observed during the first run of LHC with the ATLAS detector[8], and the observation of this very process has been comfirmed by the CMS[9] collaboration during the second run of LHC in 2018[10], while the observation of $EW\ ZZjj$ channel has been reported in 2019[11]. Inspite the endeavour has been put on the VBS process, the model-independent measurement of the differencial cross section have not been made so far.

With a total of 139 fb^{-1} proton proton collision data at $\sqrt{s} = 13$ TeV acummulated in the ATLAS detector[12] during the second run of the LHC, a great opportunity to scrutinise the SM at much higher accuracy has been provided. In this report, the fiducial differencial cross section of $ZZjj$ process measured at $\sqrt{s} = 13$ TeV using the whole run II data is reported and the results has been used to constrain a BSM effective field theory[13] which provides alternative Higgs boson interactions, vector boson interactions and additional source of CP violation in the electroweak sector.

2 Recap

In the last semester[14], an iterative unfolding procedure to remove the detector effect[15] was performed on the data corresponding to an integrated luminosity of 36 fb^{-1} using the ATLAS detector in a VBS enhanced fiducial phase space. Three distributions which is possibly sensitive to the BSM physics effect were unfolded, namely $\Delta\phi_{jj}$, M_{jj} and M_{4l}, detailed discussion on these observables can be found in section 3.4. The unfolding procedure also gives the covarience matrices which take the bin to bin migration in to account. With these infrastrctures in hand, the differencial cross section in various distributions can be easily measured and the constraints on BSM physics theories can be set using the covarience matrices and the corresponding differencial cross section, the detail of which will be discussed in section 4.3.

3 ZZjj differencial cross section

3.1 ZZjj processes and backgounds

The ATLAS detector in the LHC is a layered designed general-perpose particle detrector, the technical detail of which can be found in Ref. [12]. The detector signitures of $VVjj$ events in the ATLAS detector have a variaties of patterns, which

depend on the kind of final state vector bosons, namely W or Z boson; and the decay channel of them[16]. $ZZjj$ events with both Z bosons decay leptonically are denoted $ZZjj4l$, which is the selected channel in this analysis. Although the branching ratio for both Z bosons decay leptonically is around 10^{-3}[17], the channel has minimal hardronic backgound and no missing momenta.

At the leading order, the $ZZjj4l$ events can be separated to two categories, the electroweak production with six electroweak vertices ($EW\ ZZjj4l$), and the QCD production including two strong-interaction vertices and four electroweak vertices ($QCD\ ZZjj4l$), at the current energy scale, the $QCD\ ZZjj4l$ production has a cross section approximately 100 times larger than the cross section of EW production, which is around 1 fb. The $QCD\ ZZjj4l$ can be further separated by the initial species of initial partons, if both initial partons are gluon, the process is classified as $ggZZ4l$, otherwise classified as $qqZZ4l$. Some example leading order feynman diagrams of these processes are shown in Fig. 1.

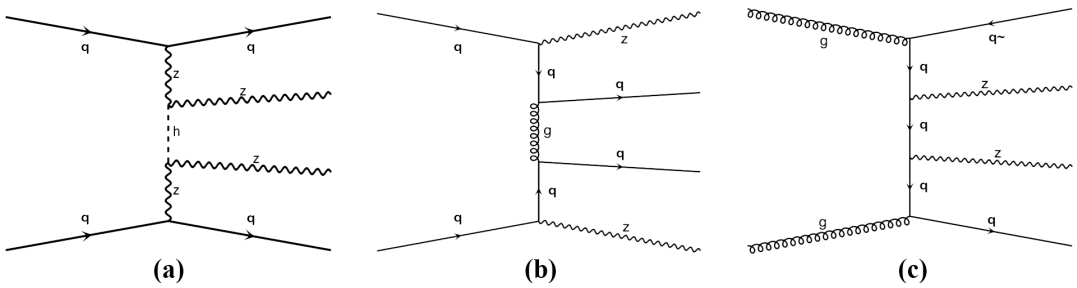

Figure 1. The leading order SM feynman diagrams contributing to $ZZjj$ processes. **(a)** $EW\ ZZjj$ process, **(b)** $QCD\ qqZZjj$ process and **(c)** is $QCD\ ggZZjj$ process.

In addition to the large $QCD\ ZZjj$ background, other non-ZZjj processes may produce the same or similar final states as the VBS processes, these background processes can therefore mimic the detector signiture of VBS process. non-ZZjj backgound processes considered in this analysis are: the production of one vector boson plus a Higgs boson, the Higgs boson then decay to four charged leptons ($VH4l$); the production of three vector bosons (VVV); and the production of two charged leptons and a pair of $t\bar{t}$ quarks ($ttll$), the top quarks decay via W bosons give birth to another pair of charged leptons. All three backgrounds are order six pure EW processes at leading order. The example feynman diagrams of these processes at leading order are shown in Fig. 2. Contribution of other processes in the studied phase space can be neglected.

Despite the extreme rarity and enormous backgound of $EW\ ZZjj4l$ process, there exist region in the phase space where the $EW\ ZZjj4l$ is enhanced while other background processes are suppressed. With $36fb^{-1}$ of data, the significance of the $EW\ ZZjj4l$ process was measured to be 1.5σ, detialed discussion can be found in my first semester report[14].

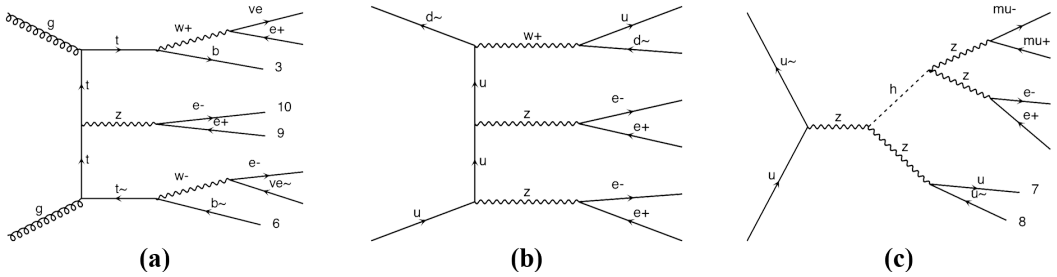

Figure 2. The leading order SM feynman diagrams contributing to non-ZZjj backgound processes, subsequent decay of the intermediate particles are also shown. **(a)** $ttll$ process, **(b)** ZZW^+ process and **(c)** ZH process.

3.2 Data and simulations

This analysis is performed using the proton proton collision data recorded in the ATLAS detector during the run II of LHC with centre-of-mass energy $\sqrt{s} = 13\ TeV$. These events were required to pass the online trigger system[18], which have an overall efficiency of 96% to 99%[19]. The total accumulated data sample corresponding to an integrated luminosity of 139 fb^{-1} is used in this analysis.

Monte Carlo (MC) Simulated events[20] are used in this analysis to correct the detector-level events for detector effects, and to estimate the expected contribution of signal and background processes. The ATLAS collaboration have switched to a newer version of software to generate MC simulations, which gives better Next-to-Leading-Order (NLO) estimations and updated jets reconstruction algorithm compared to MC simulations used last semester[14].

The $EW\ ZZjj4l$ process with no on-shell Higgs boson intermediate state was modeled by the Sherpa 2.2.2[21] event generator with NNPDF3.0NNLO parton distribution functions (PDF)[22] at leading order (LO), parton showering was handled by the Sherpa CSShower[23]. The Higgs $EW\ ZZjj4l$, in other word Vector Boson Fusion (VBF), events were simulated at NLO precision in QCD using Powheg-Box[24] interfaced to Pythia 8[25] , detailed NLO correction of the VBF process can be found in Ref. [26]. For $gg \to H \to ZZ \to 4l$ events, Powheg-Box event generator and similar NLO precision QCD estimation[27] was chosen. Other $ggZZ4l$ processes were modeled using Sherpa 2.2.2 with NNPDF3.0NNLO PDF at LO, the results were merged with CSShower parton showering. The $QCDqqZZ4l$ events were also modelled separated, $t\bar{t} \to H \to ZZ \to 4l$ events were generated at NLO[28] using Powheg-Box, while other $qqZZ4l$ events were modelled by Sherpa 2.2.2 generator with NNPDF3.0NNLO PDF at LO, and CSShower parton showering was used to model hardronization of final state quarks. The VH background events were generated at NLO precision with MiNLO[29] using Powheg-Box event generator with NNPDF3.0 PDF and Pythia 8 showering. The VVV and $ttll$ processes were modelled by Sherpa 2.2.2 with NNPDF3.0NNLO PDF at LO.

Each particle-level MC simulation event then go through detailed ATLAS detector simulation[30] based on GEANT 4[31] to produce detector-level simulation event. The detector simulation of Every processes gives three "generations" of simulation files, each generation corresponds to a specific detector status, neighbouring bunch crossings (pile-up), integrated luminosity in one year of operation of the LHC.

3.3 Event selection

Object	fiducial region
Electrons	"Loose" ID criterion "FixedCutPflowLoose" criterion $p_T > 7$ GeV, $\|\eta\| < 2.47$ $\|d_0/\sigma_{d_0}\| < 5,\ \|z_0 \times sin\theta\| < 0.5$ mm
Muons	"Loose" ID criterion "FixedCutPflowLoose" criterion $p_T > 7$ GeV, $\|\eta\| < 2.7$ $\|d_0/\sigma_{d_0}\| < 3,\ \|z_0 \times \sin\theta\| < 0.5$mm
Jets	$P_T > 30$ GeV and $Jvt > 0.6$ for $\|\eta\| < 2.4$ $P_T > 40$ GeV for $2.4 < \|\eta\| < 4.5$
OCSF lepton pairs	two pairs of OCSF lepton with M_Z closest to Z mass $p_T > 20, 20, 10$ GeV for leading 3 leptons $\Delta R_{l^+l^-} > 0.2$ 70 GeV $< M_Z <$ 110 GeV
Dijets system	leading two jets with $y_{j_1} \times y_{j_2} < 0$ and $\|y_{j_1} - y_{j_2}\| > 2$ dijet invariant mass $M_{jj} > 200$ GeV
ZZjj system	$P_T\ balance < 0.5$

Table 1. Summary of selections applied to both simulations and observaed events.

The selection of $jj4l$ events relies on the final state particles of the ZZjj4l processes, namely electrons, muons and jets.

Electrons were identified by the energy deposite in the electromagnetic calorimeter with corresponding tracks in the inner tracking detector (ID). Muons were reconstructed by the tracks in the muon spectrumeter (MS) matched to tracks in the ID, muons can also be identified by the MS alone in the region where the ID do not cover. Jets are clustered by the energy deposite in the hardronic calorimeter using the particle flow (PFlow)[32] algorithm.

The selecting criterions are largely unchanged from last semester, which can be found in Ref. [14], the only differences are that last semester one of the Z boson

can be off-shell, this time the mass of the second pair of Opposite Charge, Same Flavour (OCSF) lepton pair was required to have an invarient mass above 70 GeV, which means both Z bosons are on-shell Z boson, and a jet vertex tagger (Jvt)[33] was applied to jets with $|\eta| < 2.4$ this semester to select jets with higher possibility come from hard interactions. The selection requirements applied are summarised in T able 1, definitions of abbriveations and symbols can be found in Ref. [14].

Both the predicted particle-level and detector-level SM events were required to satisfy all criterions listed above, apart from selections that not appliable to particle-level events, for example, the lepton ID criterion and Jvt selection. The real world data events were required to pass the same selections as well. The selection of the BSM EFT particle-level events were done using the Rivet[34] framework and the jets reconstruction algorithm chosen was $anti - k_t$[35] with radius parameter $R = 0.4$, other criterions were the same as the SM particle-level selections.

Observed and SM predicted event yields in the fiducial region are listed in Table 2, where the "Other" row denotes the overall contribution of VVV, VH and $ttll$ processes. The observed event yield shows no significant deviation from the SM prediction. The significance of EW ZZjj process is measured to be 2.18σ, which corresponds to a p-value $= 8.7 \times 10^{-4}$. Some selections, for example M_{jj} were deliberately rised or abolished compared to last semester[14] to let more QCD ZZjj events into the fiducial region, which is essential for BSM physics models limit setting, details will be discussed in section 4.3.

Process	Events yield
EW ZZjj4l	22.9 ± 0.1
QCD qqZZ4l	101.3 ± 0.5
QCD ggZZ4l	26.9 ± 0.2
Other	7.9 ± 0.1
Total	158.9 ± 0.6
Data	164

Table 2. SM predicted and observed ficucial event yields for different processes. Uncertainties quoted are statistical only.

3.4 Chosen Observables

To be sensitive to CP-odd BSM physics model, the distributions of observables selected should be sensitive to CP-violating effects; in this analysis, several CP-sensitive observables have been investegated.

The most powerful observable in probing CP violation is the azimuthal angle between the leading and subleading jets[36],

$$\Delta\phi_{jj} = \phi_1 - \phi_2 \tag{3.1}$$

where the ordering of jets is determined by the rapidity of them, so that j_1 is the jet with higher rapidity (more forward in space). By artifically selecting one direction, the $\Delta\phi_{jj}$ is by definition sensitive to the Parity operator[37]. The other chosen observable, $theta_1$[38], is defined as the angle between the leading Z boson and the third lepton measured in the ZZ rest frame, i.e.

$$\theta_1 = \cos^{-1}\left(\frac{\boldsymbol{Z_1}\cdot\boldsymbol{l_3}}{|\boldsymbol{Z_1}||\boldsymbol{l_3}|}\right) \tag{3.2}$$

where the bold character denotes the three-vector of particles in ZZ rest frame. Other observables mentioned in Ref. [38] were investigated as well, but θ_1 was chosen for its best sensitivity to BSM EFT operators, more on that in section 4.3.

These distribution were initially fine binned and later re-binned to variable bin sizes, the bin width were determined by requiring at least 14 expected detector-level $ZZjj$ events each bin. Expected and observed detector-level event yields as functions of the two selected observables are shown in Fig. 3. The observation is compatible with the SM predictions.

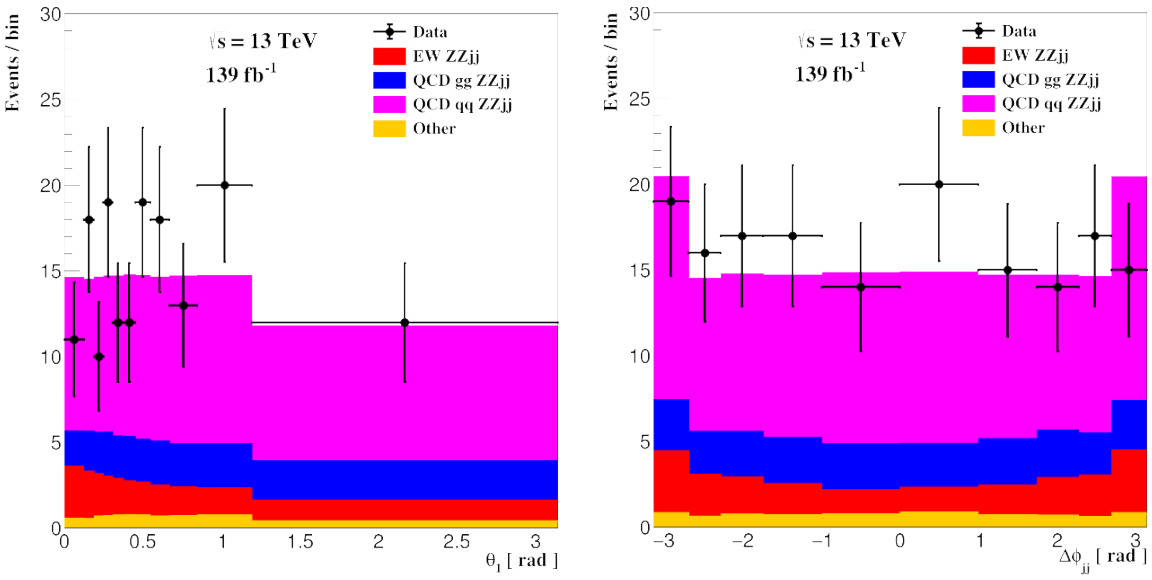

Figure 3. observed and expected event yield as function of θ_1 and $\Delta\phi_{jj}$ with variable bin width.

3.5 Unfolding

The measured $\Delta\phi_{jj}$ and θ_1 spectra were unfolded to remove detector effects, including the efficiency of trigger system, and limited resolution and efficiency of tracking detectors and calorimeters[39]. In the mean time, unfolding procedure also gives the covarience matrices account for the corralation between bins in a given distribution. By performing such correction, the results become model-independent so that they can be directly compared with particle-level predictions.

The unfolding procedure relies on the thourogh understanding to the ATLAS detector, in other word, how would a particle-level final state particles interact with the detector and what detector-level signals are expected. The imperfection of the detector results in events migration, fake signals and missing particles. Since the direct access to particle-level events is impossible, those three effects are estimated by the particle-level and detector-level simulations and represented by a respond matrix R_{ij}, more details can be found in Ref. [14]. An iterative unfolding algorithm[15] using the particle-level predicted distributions as initial hypothesis, implemented by RooUnfold framework[40] was used to achieve the unfolding. One iteration was found to be a good balance between bias and statistical uncertainties for both distributions.

Before the unfolding procedure, the non-ZZjj backgound contributions were removed from the observed data, leaving only ZZjj contributions; the faked events were then removed and the iterative method was performed; finally, a bin-by-bin efficiency correction was applied.

3.6 Results

After applying the unfolding technique, the event yields can be easily be reinterpreted to differencial cross section in the fiducial region. The measured and expected fiducial differencial cross section as function of selected observables are shown in Fig. 4, showing no significant deviation from the SM predictions

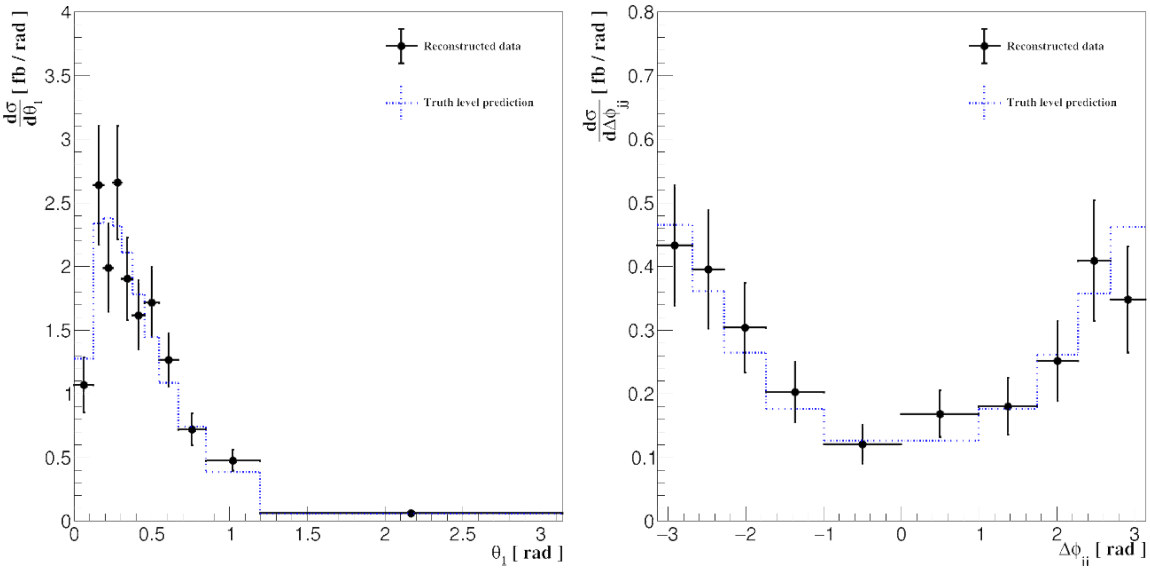

Figure 4. observed and expected event yield as function of θ_1 and $\Delta\phi_{jj}$ with variable bin width.

4 Reinterpretation in an effective field theory

4.1 EFT theory

In the SM, no CP-violation is predicted in the electroweak interactions, however, as stated, the SM is incomplete. In the SMEFT, the SM is treated as a low-energy (infrared) leading order approximation of a yet to be determined grand theory when new physics phenomena reside in a much higher energy scale, in this case, $\Lambda >> \bar{v}_T$. One can expend the SM by constructing series of expansion in the order of the ratio to new physics scale. With the SM Lagrangian defined in Ref. [41], the EFT Lagrangian constructed using $SU(3) \times SU(2) \times U(1)$ symmetry with higher dimensional BSM operators can be written as

$$\mathcal{L}_{EFT} = \mathcal{L}_{SM} + \mathcal{L}^{(6)}, \quad \mathcal{L}^{(6)} = \sum_i \frac{c_i}{\Lambda^2}\mathcal{O}_i \tag{4.1}$$

where c_i is the Wilson coefficient and $\mathcal{O}_i$ is the corresponding dimension-6 BSM operator, higher dimentional Lagrangian was neglected. The structure of the Lagrangian allows us to split the quantum amplitude, square of matrix element, to the SM and BSM part, i.e.

$$|\mathcal{M}|^2 = |\mathcal{M}_{SM}|^2 + 2\mathrm{Re}(\mathcal{M}^\dagger_{SM}\mathcal{M}_{EFT}) + |\mathcal{M}_{EFT}|^2 + \mathcal{O}(\Lambda^{-6}) \tag{4.2}$$

where $2\mathrm{Re}(\mathcal{M}^\dagger_{SM}\mathcal{M}_{EFT})$ is proportional to Λ^{-2}, which corresponds to the interferance between the SM and EFT, and $|\mathcal{M}_{EFT}|^2$ is proportional to Λ^{-4}, which is the direct EFT contribution. In this report, only one BSM operator is discuss at a time, so we hereby denote the cross section corresponding to each components of the amplitude

$$\sigma_{EFT}(C) = \sigma_{SM} + \frac{C}{\Lambda^2}\sigma_{Linear} + \frac{C^2}{\Lambda^4}\sigma_{Quad} \tag{4.3}$$

where the *Quad* and *Linear* indecate the corresponding cross section are proportional to c^2 and c respectively.

The VBS process typically contains VVV, HVV and Vqq interaction vertices, EFT operators provides alternative interactions to these vertices, for example, by exchanging unknown massive fermion whose mass is much higher than the Higgs boson. Studied EFT operators are summarised in Table 3, in which the ψ is the Higgs field, W and B are the $SU(3) \times SU(2) \times U(1)$ electroweak field tensor and τ^I is the generator of $SU(2)$ symmetry group. The operators with $\tilde{W}^I_{\mu\nu} = \epsilon^{IJK}W^{JK}_{\mu\nu}/2$ provide CP-violating effect trough the interference with the SM, while the operators without tilde are CP-even. For CP-odd operators, the integrated σ_{Linear} vanish[42] so that can only be probed by CP-sensitive observables, whereas the σ_{Quad} can be probed by the total cross section deviation from the SM prediction.

Coefficient	Operator	Relavent vertices
c_W	$\epsilon^{IJK} W^{I,\nu}_{\mu} W^{J,\rho}_{\nu} W^{K,\mu}_{\rho}$	VVV
$c_{\tilde{W}}$	$\epsilon^{IJK} \tilde{W}^{I,\nu}_{\mu} W^{J,\rho}_{\nu} W^{K,\mu}_{\rho}$	VVV
c_{HW}	$\psi^{\dagger}\psi W^{I}_{\mu\nu} W^{I,\mu\nu}$	HVV
$c_{H\tilde{W}}$	$\psi^{\dagger}\psi \tilde{W}^{I}_{\mu\nu} W^{I,\mu\nu}$	HVV
c_{HWB}	$\psi^{\dagger}\tau^{I}\psi W^{I}_{\mu\nu} B^{\mu\nu}$	HVV and Vqq
$c_{H\tilde{W}B}$	$\psi^{\dagger}\tau^{I}\psi \tilde{W}^{I}_{\mu\nu} B^{\mu\nu}$	HVV and Vqq

Table 3. Studied Wilson coefficients and the corresponding operators and the interaction vertices they alter.

4.2 particle-level EFT event generation

The parton-level EW ZZjj EFT events were generated at center-of-mass energy of 13 TeV using MADGRAPH 5[43] event generator, with the SMEFTsim[13] EFT implimentation. The chosen SMEFTsim package is a simplified $U(3)^5$ EFT model which dramatically reduces the number of Wilson coefficients (69[13] versus 2499 for full SMEFT[44]) thus reduces the need for computation power. The $\{M_W, M_Z, G_F\}$ input scheme was chosen for certain theoretical advantages and better precision over the $\{\alpha_{EW}, M_Z, G_F\}$ input scheme[13]. The parton-level results were then passed to PYTHIA 8[25] to model the decay of Z boson and the hardronization of final state quarks. The particle-level events then go through the same selections described in section 3.3. The EFT events the selections were reimplimented using the RIVET framework[34].

The linear and quadratic EFT events of EW jj4l process were generated separately with only one Wilson coefficient set to $c = 5$, while others set to zero, and $\Lambda = 1$ TeV. One can simply scale the resulting spectra by the proportional rule for σ_{Linear} and σ_{Quad}, see equation 4.3, to get distributions corresponding to other values of the Wilson coefficient.

Due to the limitation of computing resources, I am not able to generate adequate EW jj4l events to minimise the statistical fluctuation. As a result only processes with two on-shell Z bosons were generated to keep generating time resonable. The predicted SM differencial cross-sections as function of $\Delta\phi_{jj}$ generated with and without the off-shell Z boson in the fiducial region are shown in Fig. 5, indicating little difference between the two samples in the fiducial region.

In fig. 6 and 7, the ratio of EFT differencial cross section with $C = 1$ as function of $\Delta\phi_{jj}$ and θ_1 to the SM prediction are shown. the $\Delta\phi_{jj}$ spectrum shows excellent sensitivity to the CP-odd EFT operators, and θ_1 spectrum shows great sensitivity to CP-even EFT operators. The largest EFT effect is the contributions corresponding to Wilson coefficients C_W and $C_{\tilde{W}}$, while little sensitivities were shown for C_{HWB} and $C_{H\tilde{W}B}$. To quantify the inclusive CP-violation, a geometrical asymmetry A is

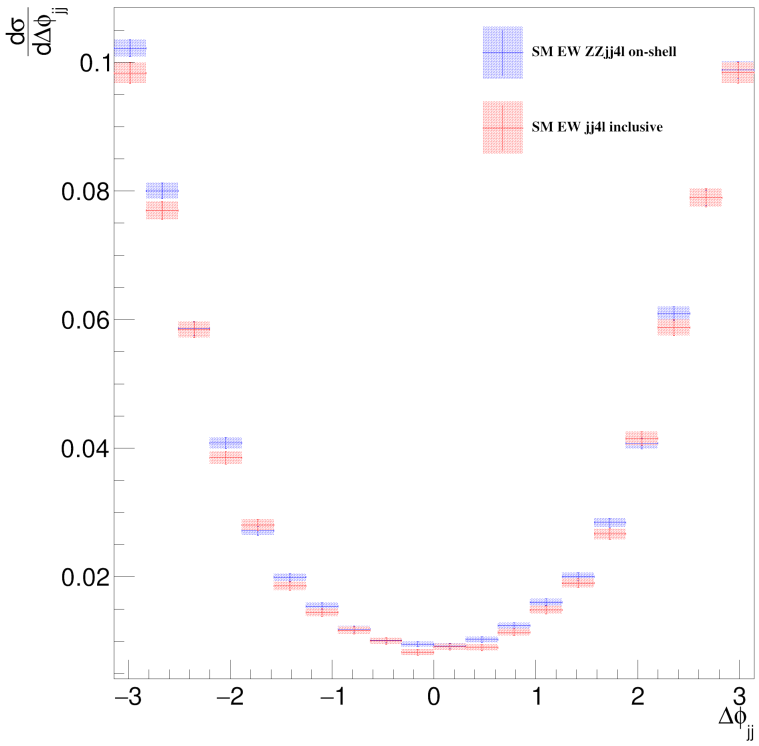

Figure 5. The predicted SM differencial cross-section as function of $\Delta\phi_{jj}$ generated with and without the off-shell Z boson in the fiducial region, indicating no obvious mismodelling by not generating processes with off-shell Z bosons.

defined as

$$A = \frac{\sigma_+ - \sigma_-}{\sigma_+ + \sigma_-} \tag{4.4}$$

where $\sigma_\pm$ is the cross section in the positive and negative $\Delta\phi_{jj}$ part in the fiducial region. The change of fiducial cross sections and induced Asymmetries by each EFT operator with $C = 1$ are summarised in Table 4, indicating the CP-odd operators do not affect the total cross section at Linear order but do have contribution to Asymmetry. Note that at $C = 1$ the quadratic contributions are similar to the linear contributions, at larger Wilson coefficient the quadratic correction can dominate the EFT effect.

4.3 Limit setting procedure

With relatively high observed statistics in each bin of the two studied distributions, the uncertainties can be modelled by Gaussian. The χ^2 function constructed to set limits on the Wilson coefficients is defined as

$$\chi^2 = (\overrightarrow{\sigma}_{data} - \overrightarrow{\sigma}_{EFT})^T \mathbf{Cov}^{-1} (\overrightarrow{\sigma}_{data} - \overrightarrow{\sigma}_{EFT}) \tag{4.5}$$

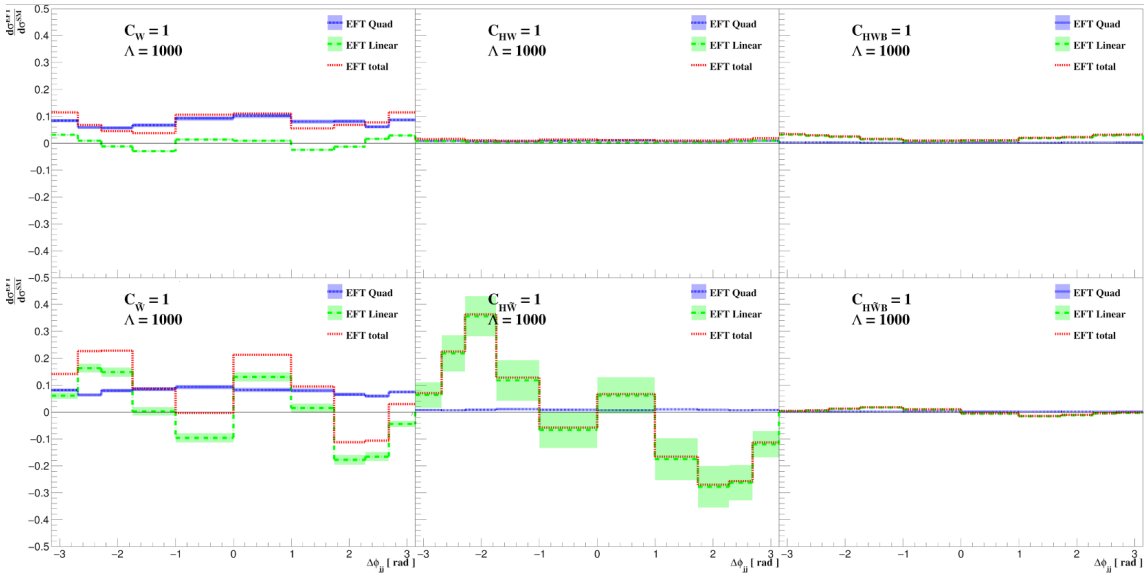

Figure 6. The ratio of EFT differencial cross section with $C = 1$ as function of $\Delta\phi_{jj}$ to the SM predicted cross sections, showing that the $\Delta\phi_{jj}$ spectrum have great sensitivity to CP-odd EFT operators.

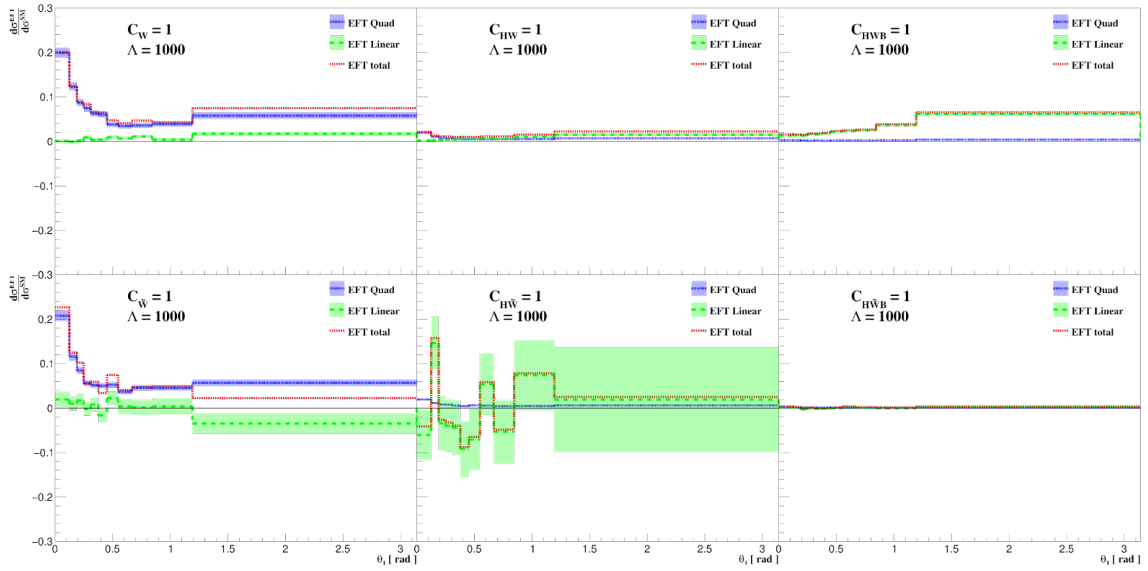

Figure 7. The ratio of EFT differencial cross section with $C = 1$ as function of θ_1 to the SM predicted cross sections, showing that the θ_1 spectrum have great sensitivity to CP-even EFT operators.

where $\overrightarrow{\sigma}_{data}$ and $\overrightarrow{\sigma}_{EFT}$ are the vectors of observed and predicted EFT cross section in every bins of a particular distribution, **Cov** is the statistical covarience matrix given by the the unfolding procedure. Each time two of the Wilson coefficients C_1, C_2 was scaned and a pair of $\{C_1^{min}, C_2^{min}\}$ which minimise the χ^2 was determined.

Type	σ_{Linear} [fb]	σ_{Quad} [fb]	σ_{EFT}/σ_{SM}	Asymmetry
SM	-	-	-	0.002 ± 0.003
c_W	0.008 ± 0.002	0.119 ± 0.004	0.082 ± 0.003	0.003 ± 0.003
$c_{\tilde{W}}$	0.006 ± 0.008	0.117 ± 0.004	0.080 ± 0.006	-0.059 ± 0.006
c_{HW}	0.0083 ± 0.0005	0.0117 ± 0.0003	0.0130 ± 0.0004	-0.002 ± 0.003
$c_{H\tilde{W}}$	-0.02 ± 0.03	0.0117 ± 0.0003	-0.00 ± 0.02	-0.15 ± 0.02
c_{HWB}	0.0342 ± 0.0008	0.00313 ± 0.00007	0.0242 ± 0.0005	-0.002 ± 0.003
$c_{H\tilde{W}B}$	0.0002 ± 0.0007	0.00175 ± 0.00004	0.0012 ± 0.0005	-0.010 ± 0.003

Table 4. The predicted particle level EFT fiducial cross section, their ratio to the SM prediction and the Asymmetries at $C = 1$ and $\Lambda = 1$ TeV. The uncertainties quoted are statistical only.

The $\Delta\chi^2$ was then constructed by

$$\Delta\chi^2(C_1, C_2) = \chi^2(C_1, C_2) - \chi^2_{min} \tag{4.6}$$

According to the Wilk's theorm[45], the $\Delta\chi^2$ also follows the χ^2 distribution, whose corresponding Number of Degrees of Freedom (NDF) equals the remaining free parameters, in this case 2. The Confidence Level (CL) of each point on the plane was calculated by

$$1 - CL = \int_{\Delta\chi^2}^{\infty} f_{k=2}(x)dx \tag{4.7}$$

where the χ^2_{min} is the minimum χ^2 on the plane and $f_k(x)$ is the χ^2 distribution function with NDF $k = 2$.

4.4 Results

The 68% and 95% expected and observed limits on two of the studied CP-odd Wilson coefficients with other coefficients set to 0 calculated using the $\Delta\phi_{jj}$ distribution are shown in the left panel right panels in Figure 8, the asymmetries on the plane are also overlayed. The observed $\Delta\chi^2$ are shown in the left panels.

The 68% and 95% expected and observed limits on two of the studied CP-even Wilson coefficients with other coefficients set to 0 calculated using the θ_1 distribution are shown in the left panel right panels in Figures 9. The observed $\Delta\chi^2$ are shown in the left panels.

The one-dimensional observed and expected constraints of individual Wilson coefficient are also calculated, in this case the NDF of the $\Delta\chi^2$ distribution was set to 1, so that the resulting limit are quite tighter than the two-dimensional limits. The results are summarised in Table 5. As expected, the $\Delta\phi_{jj}$ distribution is more sensitive to CP-odd operators whereas the θ_1 distribution gives tighter limits on CP-even Wilson coefficients.

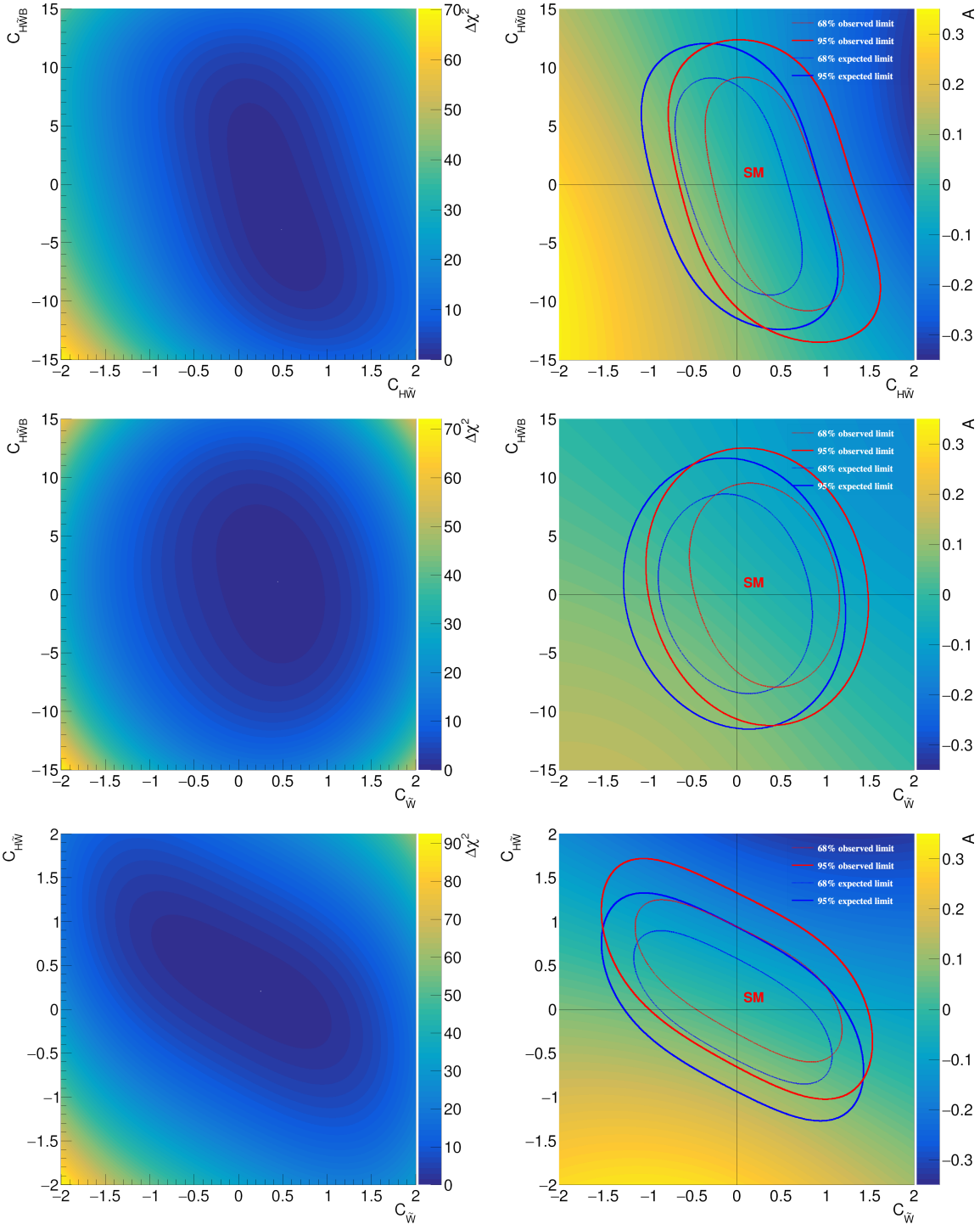

Figure 8. *TODO*

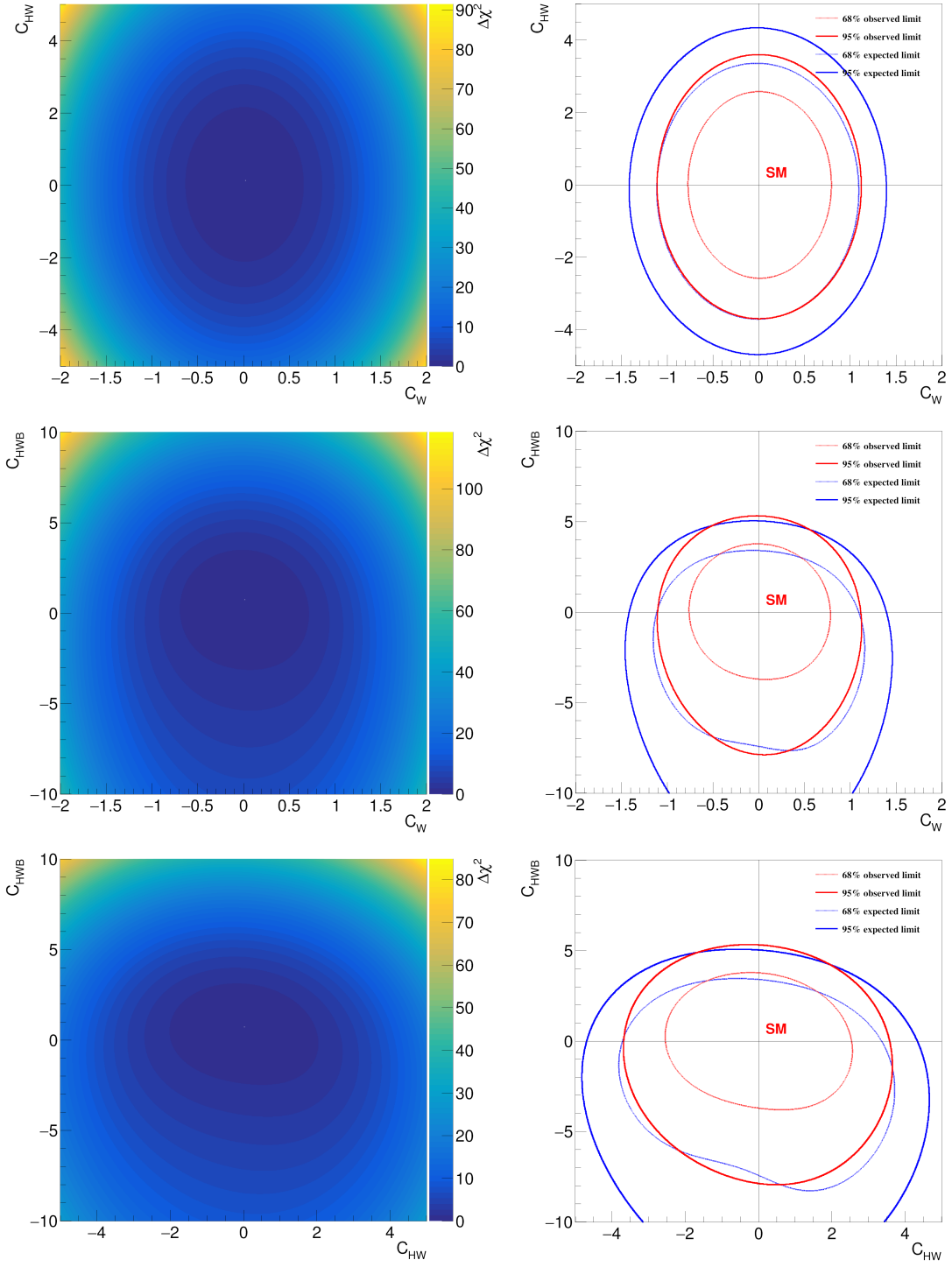

Figure 9. *TODO*

5 Discussion

The process of EW ZZjj with on-shell Z bosons shows good sensitivity to selected EFT operators in the fiducial region. Compared to the $H \to Z^*Z \to 4l$ process[36],

Coeff.	Distro.	68% obs.	95% obs.	68% exp.	95% exp.
C_W	θ_1	[-0.37, 0.41]	[-0.66, 0.68]	[-0.64, 0.62]	[-0.89, 0.88]
	$\Delta\phi_{jj}$	[-0.80, 0.39]	[-1.06, 0.82]	[-0.72, 0.65]	[-1.01, 0.94]
$C_{\tilde{W}}$	θ_1	[-0.41, 0.36]	[-0.69, 0.63]	[-0.64, 0.58]	[-0.90, 0.84]
	$\Delta\phi_{jj}$	[-0.06, 0.56]	[-0.38, 0.81]	[-0.31, 0.31]	[-0.59, 0.58]
C_{HW}	θ_1	[-1.24, 1.33]	[-2.22, 2.17]	[-2.16, 1.83]	[-3.01, 2.66]
	$\Delta\phi_{jj}$	[-2.78, 1.55]	[-3.65, 2.67]	[-2.62, 1.94]	[-3.53, 2.85]
$C_{H\tilde{W}}$	θ_1	[0.30, 0.99]	[-0.03, 1.33]	[-0.32, 0.33]	[-0.64, 0.65]
	$\Delta\phi_{jj}$	[-0.03, 0.37]	[-0.23, 0.57]	[-0.19, 0.19]	[-0.37, 0.38]
C_{HWB}	θ_1	[-0.96, 1.62]	[-2.58, 2.65]	[-1.54, 1.28]	[-3.55, 2.35]
	$\Delta\phi_{jj}$	[-11.4, 1.06]	[-13.1, 2.35]	[-2.04, 1.51]	[-11.9, 2.72]
$C_{H\tilde{W}B}$	θ_1	[-2.17, 4.60]	[-5.24, 6.68]	[-5.52, 5.18]	[-7.79, 7.44]
	$\Delta\phi_{jj}$	[-2.38, 4.96]	[-5.51, 7.35]	[-3.52, 3.58]	[-6.14, 6.24]

Table 5. *todo*

constraints on operators corresponding to C_HW, $C_{H\tilde{W}}$ and C_{HWB}, $C_{H\tilde{W}B}$ are tighter. The model independent technique shows good robustness and the CP-sensitive observables are proved useful.

However, there are a few limitations. Firstly, although large set of EFT events were generated, due to the low branching ratio only around 2000 events were eventrally selected in the fiducial region, which can lead to rather large statistical fluctuations. These uncertainties were not taken into account in the limit setting procedure.

Secondly, only statistical uncertainties were considered, systematical and theoretical uncertainties in both EFT and SM distributions were not taken into account. Lower sensitivities are expected if these uncertainties are be considered.

Thirdly, The NDF of the χ_2 distributions should be determined experimentally using large sets of psudo-experiments, but in this analysis they are set to 1 or 2 depending on the number of envolved Wilson coefficients.

Finally, if more than one Wilson coefficients were non-zero values, the Λ^{-4} correction to the cross section should also contain the interference between these Wilson coefficients, which can only be ignored when C_1C_2/Λ^{-4} is small compared to other Λ^{-4} contributions, in other word one of the involving Wilson coefficients is small compared to the other one, but was ignored regardlessly in this report.

Future development of this analysis can be carried out based on these limitations, constraints on other new physics model can also be easily estimated using similar technique.

References

[1] M. K. Gaillard, P. D. Grannis and F. J. Sciulli, *The standard model of particle physics*, *Rev. Mod. Phys.* **71** (1999) S96–S111.

[2] L. Canetti, M. Drewes and M. Shaposhnikov, *Matter and antimatter in the universe*, *New J. Phys.* **14** (2012) 095012.

[3] L. Evans and P. Bryant, *LHC machine*, *J. Instrum.* **3** (2008) S08001.

[4] G. Aad and et al., *Observation of a new particle in the search for the Standard Model Higgs boson with the ATLAS detector at the LHC*, *Phys. Lett. B* **716** (2012) 1–29.

[5] M. Rauch, *Vector-Boson Fusion and Vector-Boson Scattering*, 2016.

[6] S. Dawson, *Introduction to Electroweak Symmetry Breaking*, 1999.

[7] R. D. Peccei, *CP Violation: A Theoretical Review*, 1995.

[8] G. Aad, B. Abbott and et al., *Evidence for Electroweak Production of $W^{\pm}W^{\pm}jj$ in pp Collisions at $\sqrt{s} = 8$ TeV with the ATLAS detector*, *Phys. Rev. Lett.* **113** (2014) .

[9] CMS collaboration, *The CMS Experiment at the CERN LHC*, *J. Instrum.* **3** (2008) S08004.

[10] A. Sirunyan and et al., *Observation of electroweak production of same-sign w boson pairs in the two jet and two same-sign lepton final state in proton-proton collision at $\sqrt{s} = 13$ TeV*, *Phys. Rev. Lett.* (2018) .

[11] ATLAS Collaboration collaboration, *Observation of electroweak production of two jets in association with a Z-boson pair in pp collisions at $\sqrt{s} = 13$ TeV with the ATLAS detector*, Tech. Rep. ATLAS-CONF-2019-033, CERN, Geneva, Jul, 2019.

[12] ATLAS collaboration, *The ATLAS Experiment at the CERN Large Hadron Collider*, *J. Instrum.* **3** (2008) S08003.

[13] I. Brivio, Y. Jiang and M. Trott, *The SMEFTsim package, theory and tools*, *J. High Energy Phys.* **2017** (2017) .

[14] D. Qichen, *Model-independent measurement of production of two jets with two charged lepton pairs in ATLAS detector at $\sqrt{s} = 13$ TeV*, .

[15] G. D'Agostini, *A Multidimensional unfolding method based on Bayes' theorem*, *Nucl. Instrum. Meth.* **A362** (1995) 487.

[16] P. Watkins, *Discovery of the W and Z boson*, *Contemp. Phys.* **27** (1986) 291.

[17] Particle Data Group collaboration, *Review of Particle Physics*, *Phys. Rev. D* **98** (2018) 030001.

[18] ATLAS Collaboration collaboration, *The Run-2 ATLAS Trigger System: Design, Performance and Plan*, Tech. Rep. ATL-DAQ-PROC-2016-039, CERN, Geneva, Dec, 2016.

[19] M. Aaboud, G. Aad, B. Abbott, O. Abdinov, B. Abeloos, D. K. Abhayasinghe et al., *Measurement of the four-lepton invariant mass spectrum in 13 tev proton-proton collisions with the atlas detector*, *Journal of High Energy Physics* **2019** (2019) .

[20] R. Y. Rubinstein and D. P. Kroese, *Simulation and the Monte Carlo Method*. Wiley Publishing, 3rd ed., 2016.

[21] P. Freeman, S. Doe and A. Siemiginowska, *<title>sherpa: a mission-independent data analysis application</title>*, *Astronomical Data Analysis* (2001) .

[22] R. D. Ball, V. Bertone, S. Carrazza, C. S. Deans, L. Del Debbio, S. Forte et al., *Parton distributions for the lhc run ii*, *Journal of High Energy Physics* **2015** (2015) .

[23] E. Bothmann, G. Singh Chahal, S. Höche, J. Krause, F. Krauss, S. Kuttimalai et al., *Event generation with sherpa 2.2*, *SciPost Physics* **7** (2019) .

[24] C. Oleari, *The powheg box*, *Nuclear Physics B - Proceedings Supplements* **205-206** (2010) 36–41.

[25] T. Sjöstrand, S. Ask, J. R. Christiansen, R. Corke, N. Desai, P. Ilten et al., *An introduction to pythia 8.2*, *Computer Physics Communications* **191** (2015) 159–177.

[26] P. Nason and C. Oleari, *Nlo higgs boson production via vector-boson fusion matched with shower in powheg*, *Journal of High Energy Physics* **2010** (2010) .

[27] S. Alioli, P. Nason, C. Oleari and E. Re, *NLO Higgs boson production via gluon fusion matched with shower in POWHEG*, *JHEP* **04** (2009) 002 [0812.0578].

[28] H. B. Hartanto, B. Jager, L. Reina and D. Wackeroth, *Higgs boson production in association with top quarks in the POWHEG BOX*, *Phys. Rev. D* **91** (2015) 094003 [1501.04498].

[29] K. Hamilton, P. Nason and G. Zanderighi, *Minlo: multi-scale improved nlo*, *Journal of High Energy Physics* **2012** (2012) .

[30] G. Aad, B. Abbott, J. Abdallah, A. A. Abdelalim, A. Abdesselam, O. Abdinov et al., *The atlas simulation infrastructure*, *The European Physical Journal C* **70** (2010) 823–874.

[31] S. Agostinelli, J. Allison, K. Amako, J. Apostolakis, H. Araujo, P. Arce et al., *Geant4—a simulation toolkit*, *Nuclear Instruments and Methods in Physics Research Section A: Accelerators, Spectrometers, Detectors and Associated Equipment* **506** (2003) 250 .

[32] M. Aaboud, G. Aad, B. Abbott, J. Abdallah, O. Abdinov, B. Abeloos et al., *Jet reconstruction and performance using particle flow with the atlas detector*, *The European Physical Journal C* **77** (2017) .

[33] T. Kehinde, *Performance of jet vertex tagger in suppression of pileup jets and E_T^{miss} in atlas detector*, *Journal of Physics: Conference Series* **802** (2017) 012012.

[34] C. Bierlich, A. Buckley, J. Butterworth, C. H. Christensen, L. Corpe, D. Grellscheid

et al., *Robust independent validation of experiment and theory: Rivet version 3*, *SciPost Physics* **8** (2020) .

[35] M. Cacciari, G. P. Salam and G. Soyez, *The anti-ktjet clustering algorithm*, *Journal of High Energy Physics* **2008** (2008) 063–063.

[36] F. U. Bernlochner, C. Englert, C. Hays, K. Lohwasser, H. Mildner, A. Pilkington et al., *Angles on cp-violation in higgs boson interactions*, *Physics Letters B* **790** (2019) 372–379.

[37] C. S. Wu, E. Ambler, R. W. Hayward, D. D. Hoppes and R. P. Hudson, *Experimental test of parity conservation in beta decay*, *Phys. Rev.* **105** (1957) 1413.

[38] S. Bolognesi, Y. Gao, A. V. Gritsan, K. Melnikov, M. Schulze, N. V. Tran et al., *Spin and parity of a single-produced resonance at the lhc*, *Physical Review D* **86** (2012) .

[39] S. Schmitt, *Data unfolding methods in high energy physics*, *EPJ Web of Conferences* **137** (2017) 11008.

[40] T. Adye, *Unfolding algorithms and tests using roounfold*, 2011.

[41] A. Salam, *Weak and Electromagnetic Interactions*, *Conf. Proc. C* **680519** (1968) 367.

[42] A. Azatov, R. Contino, C. S. Machado and F. Riva, *Helicity selection rules and noninterference for bsm amplitudes*, *Physical Review D* **95** (2017) .

[43] J. Alwall, R. Frederix, S. Frixione, V. Hirschi, F. Maltoni, O. Mattelaer et al., *The automated computation of tree-level and next-to-leading order differential cross sections, and their matching to parton shower simulations*, *Journal of High Energy Physics* **2014** (2014) .

[44] R. Alonso, E. E. Jenkins, A. V. Manohar and M. Trott, *Renormalization group evolution of the standard model dimension six operators iii: gauge coupling dependence and phenomenology*, *Journal of High Energy Physics* **2014** (2014) .

[45] S. S. Wilks, *The large-sample distribution of the likelihood ratio for testing composite hypotheses*, *Ann. Math. Statist.* **9** (1938) 60.